

Penetration of crustal melt beyond the Kunlun Fault into northern Tibet

Florian Le Pape^{1,2*}, Alan G. Jones¹, Jan Vozar¹ and Wei Wenbo³

The weak lithosphere of the Tibetan plateau is surrounded by rigid crustal blocks¹ and the transition between these regimes plays a key role in the ongoing collision between India and Eurasia. Geophysical data²⁻⁵ and magmatic evidence^{6,7} support the notion that partial melt exists within the anomalously hot^{7,8} crust of northern Tibet. The Kunlun Fault, which accommodates the plateau's eastward extrusion, has been identified as a significant rheological boundary⁴ between weak, warm Tibetan crust⁸ and the rigid eastern Kunlun–Qaidam block. Here we present reanalyses and remodelling of existing magnetotelluric data⁴, using an anisotropy code⁹ to obtain revised resistivity models. We find unequivocal evidence for anisotropy in conductivity at the northern edge of the Tibetan plateau. We interpret this anisotropy as the signature of intrusion of melt that penetrates north from the Tibetan plateau and weakens the crust beneath the Kunlun Shan. We suggest that our identification of a melt intrusion at the northern edge of the Tibetan plateau compromises the previous identification of the Kunlun Fault as an important rheological boundary. We conclude that the crustal melt penetration probably characterizes the growth of the plateau¹⁰ to the north, as well as accommodating the north–south crustal shortening in Tibet.

The International Deep Profiling of Tibet and Himalaya (INDEPTH) phase III 600-line magnetotelluric profile⁴ crosses three major tectonic complexes of the northern Tibetan plateau: the Qiangtang terrane, the Songpan–Ganzi terrane and the eastern Kunlun–Qaidam terrane, respectively separated by the Jinsha River Suture (JRS) and the Kunlun Fault (Fig. 1). Although not remarkable at the surface, the JRS has been identified as a significant crustal boundary¹¹. The Songpan–Ganzi terrane is characterized by several kilometres of a thick sequence of Triassic turbidites¹². Those flysch complexes are mostly easily deformable pelites, deposited in a deep marine setting, which were probably underthrust to lower crustal depths in the Mesozoic and along Cenozoic thrust faults, such as the Fenghuo Shan–Nangqian, localizing Tertiary contractional deformation in central–northern Tibet¹². To the north, the 1,000-km-long, east–west-trending Kunlun Fault follows the trace of the Anyimaqen–Kunlun–Muztagh suture separating the Songpan–Ganzi block from the eastern Kunlun–Qaidam block¹². Just west of the Lhasa–Golmud highway, the fault splits into the South Kunlun Fault (SKF) and the Kunlun Fault (Fig. 1). In this study, a subset of 19 long-period magnetotelluric (LMT) stations and 34 broadband magnetotelluric (BBMT) stations from the 1999 600-line survey (Fig. 1) are reanalysed and remodelled using modern techniques previously unavailable. Time series were not reprocessed⁴, but, at common locations, the BBMT and LMT data were remerged considering the LMT data as the shifting reference

for statics control. Longer periods of the transverse electric mode were not used from some sites (Supplementary Fig. S1) as they were more affected by noise and distortion owing to the effect of the highly conductive Qaidam Basin bounding the northern edge of the profile⁴. Previous inversions⁴ of the data from the 600 line used both magnetotelluric modes (transverse magnetic and transverse electric) and vertical magnetic field data to derive highly smoothed models that were all characterized by a relatively laterally uniform, mid-crustal conductor extending from the southern end of the 600-line profile to the Kunlun Shan and ending abruptly at the Kunlun Fault. The high conductivity of the middle and lower crust south of the Kunlun Shan was interpreted as partial melt, consistent with previous interpretations of INDEPTH phase II magnetotelluric data farther south^{5,13}. Our new two-dimensional (2D) anisotropic resistivity model for the 600 line fits the data better (both in global root-mean-square (RMS) misfit and in local misfits) than the previous model, is more focussed, less smooth, exhibits greater lateral variability and particularly highlights required electrical anisotropy in the northern part of the profile (Figs 2 and 3).

Here we highlight three models: global anisotropic and isotropic models of the 600 line (Fig. 2) and a local anisotropic crustal model obtained using fewer stations and focusing on the upper to middle crust around the Kunlun Shan (Fig. 3). Strike analysis and distortion decomposition¹⁴ were applied to all data to determine the most appropriate 2D profile orientation perpendicular to geo-electric strike and to correct the data for determinable galvanic effects. For all models, the geo-electric strike orientations were found to be in agreement with the east–west trend of the main geological structures. The models were obtained using a modified version⁹ of a 2D magnetotelluric inversion algorithm¹⁵ incorporating a trade-off parameter for electrical anisotropy⁹. The 2D anisotropy problem is restrictively solved by assuming that the anisotropy axes are parallel and perpendicular to the main axis of regional geo-electric strike, an assumption valid for this region but not generally applicable. Anisotropic modelling defines three models; *xx*-horizontal resistivity across-profile, *yy*-horizontal resistivity along-profile and *zz*-vertical resistivity (the *zz* model is not shown as it is very similar to *xx*). The data were inverted simultaneously for both transverse magnetic and transverse electric modes and also the geomagnetic transfer function (Supplementary Figs S1 and S2).

Both isotropic and anisotropic models are consistent on a lithospheric scale and exhibit several robust features that were not evident in the previous isotropic solutions⁴, but show significant differences in the middle–lower crust of the Kunlun Shan area. First of all, on both global and focused inversions the anisotropic modelling particularly highlights an extension of the conductive

¹Dublin Institute for Advanced Studies, 5 Merrion Square, Dublin 2, Ireland, ²National University of Ireland Galway, University Road, Galway, Ireland,

³China University of Geosciences Beijing, 29 Xueyuan Road, Beijing 100083, China. *e-mail: flepape@cp.dias.ie.

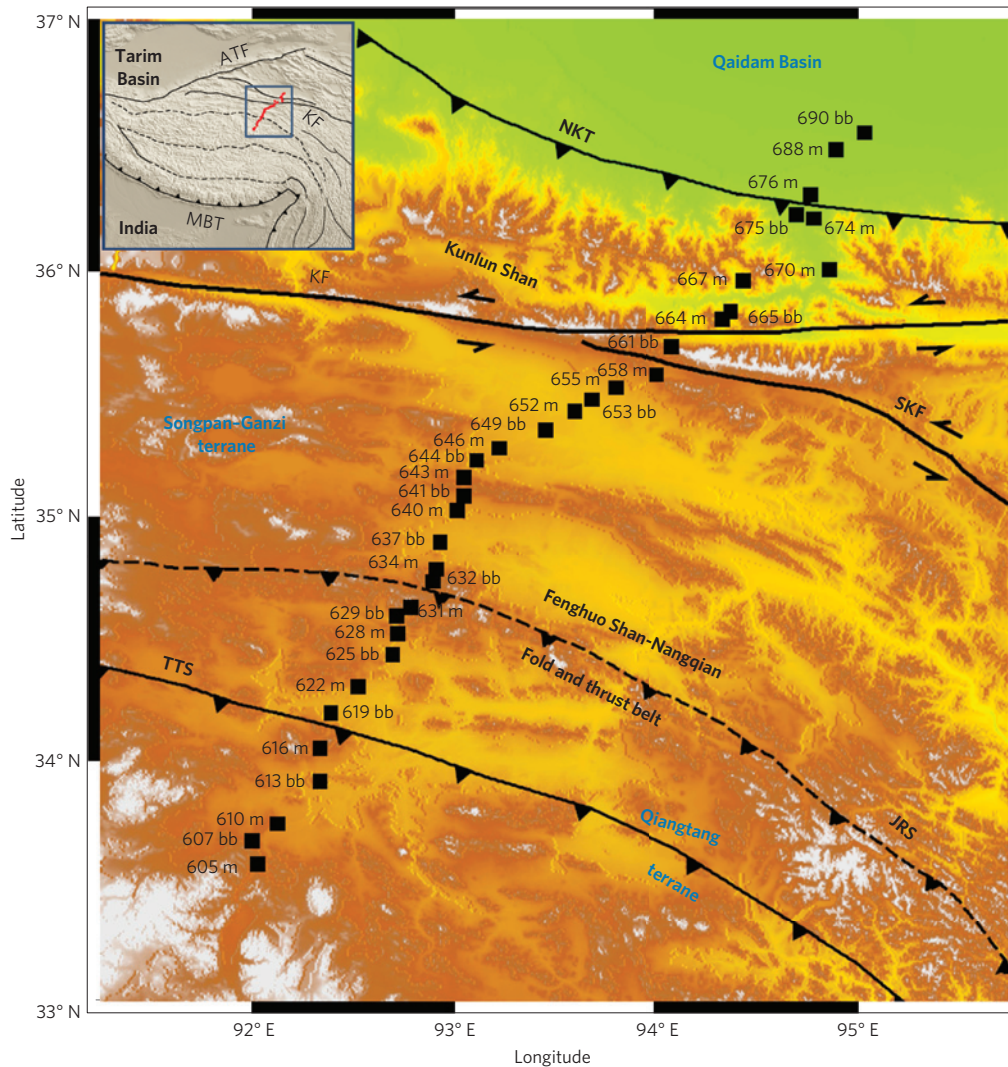


Figure 1 | Location of the 600-line magnetotelluric stations associated with the regional tectonic settings. The map shows the locations of the long-period and broadband merged stations (m) as well as broadband-only stations (bb). ATF, Altyr Tagh Fault; KF, Kunlun Fault; MBT, Main boundary thrust.

anomaly to the north in the y direction (Figs 2 and 3), that is, the profile direction perpendicular to the fault. Second, vertical offsets in the mid-crustal conductive layer south of the SKF show convincing spatial correlations with locally mapped tectonic features (Fig. 2). Furthermore, from the resistivity constraints inferred by our new model (Supplementary Fig. S3), the upper mantle is not as conductive as the crust, indicating that the upper mantle cannot contain as great a volume of interconnected melt. Finally, north of the SKF, the crust and upper mantle are far more resistive and must be characterized by colder temperatures and therefore stiffer rheological conditions. Furthermore, in the southern edge of the profile, the deeper part of the mantle (>100 km depth) is relatively resistive (Fig. 2). As the crustal conductor can reduce resolution of deeper structures, the mantle resistivity imaged by the magnetotelluric model is a minimum bound¹⁶ and the true resistivity of this particular feature is likely to be higher. However, owing to the presence of the strong crustal conductors, the deep mantle structure in the middle of the profile is not well resolved (Supplementary Fig. S3).

The partial melt characterized by high conductivity in the Qiangtang and Songpan–Ganzi crust will follow variation in surface magmatism in both space and time⁷. Eocene to Oligocene magmatism in the Qiangtang terrane is mainly associated with

reactivation of the Mesozoic Bangong and Jinsha sutures, with northward subduction of Lhasa terrane and southward subduction of Songpan–Ganzi terrane, respectively⁶. Middle-Miocene to Quaternary magmatism, although minor, is widely distributed in the Songpan–Ganzi terrane and more locally in the northern Qiangtang terrane⁶. The conductivity of a partially molten rock depends on the interconnectivity of melt, as opposed to melt insulated in pockets, and melt interconnectivity exists at low melt fractions¹⁷. Large-volume fractions of melt are not required to explain our magnetotelluric model; however, our model highlights and reconfirms that melt is widespread in the crust, as previously proposed⁵. The recent volcanism in northern Tibet, as well as the widespread crustal melting (Fig. 2), is likely to be the consequence of the southward subduction of Asian lithospheric mantle beneath the Songpan–Ganzi terrane, imaged by seismic receiver functions¹⁸, associated with convective thinning of the Tibetan mantle lithosphere^{7,18,19}. The thinning of the Tibetan lithosphere explains the widespread distribution of potassic volcanism in the Songpan–Ganzi terrane^{6,7}. Our model highlights resistive mantle at a depth of 140 km in the south of the profile, which does not agree with thin Tibetan lithosphere extending farther south of the Bangong–Nujiang suture zone¹⁸. The resistive feature is too resistive to corroborate the thin Tibetan plate¹⁸

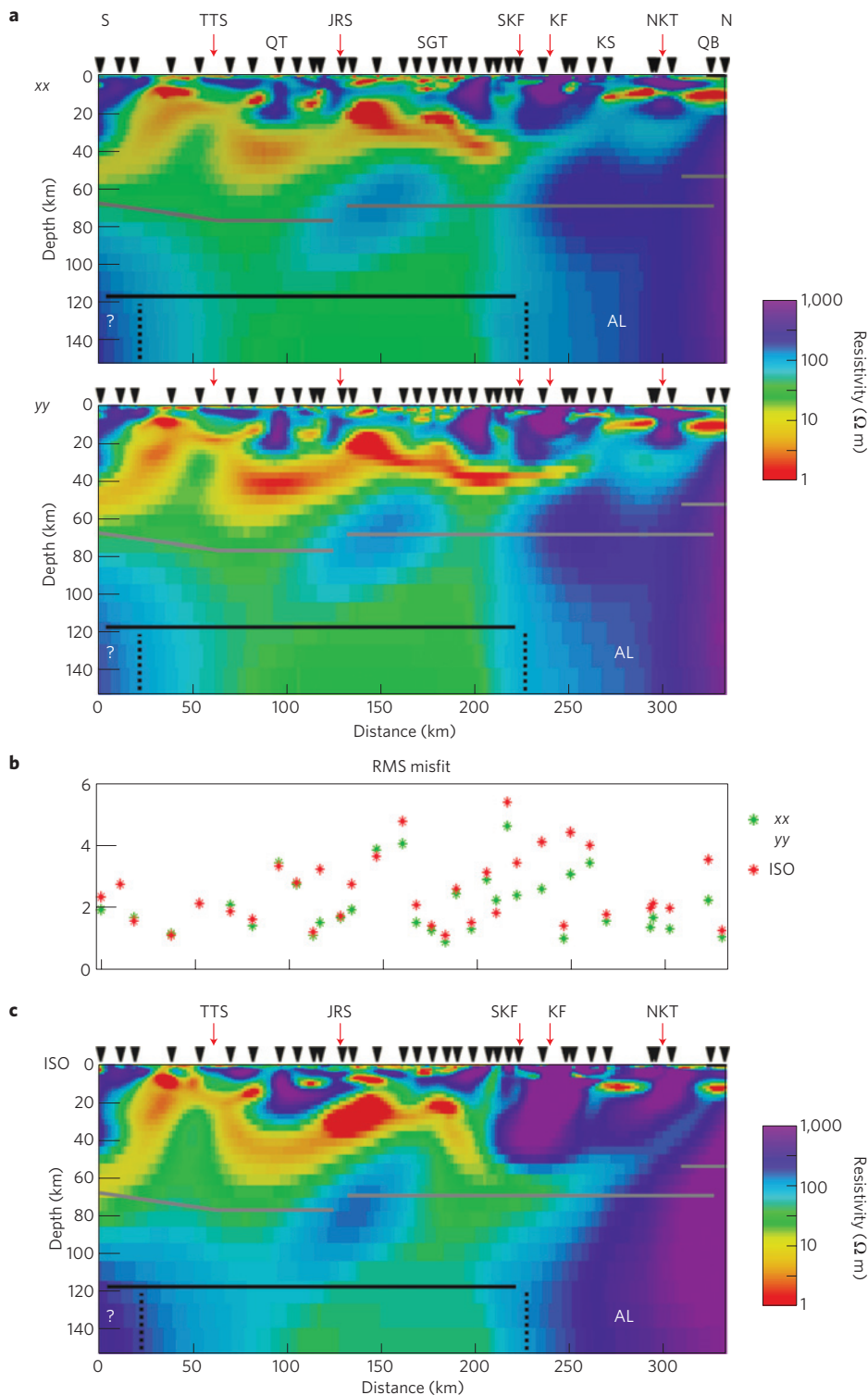


Figure 2 | Global anisotropic and isotropic 2D modelling. **a**, 2D anisotropic resistivity model. **b**, Difference between the anisotropic (green) and isotropic (ISO, red) RMS misfits. **c**, 2D isotropic resistivity model. For models **a** and **c**, the Moho depth^{21,25} is highlighted by the grey line. The black line shows the lithosphere–asthenosphere boundary location for a thin Tibetan lithosphere in the north part of the plateau imaged by seismic receiver functions¹⁸. S, south; N, north; AL, Asian lithosphere; QT, Qiangtang terrane; SGT, Songpan–Ganzi terrane; KS, Kunlun Shan; QB, Qaidam Basin; JRS, Jinsha River Suture; TTS, Tanggula thrust system; KF, Kunlun Fault.

but not deep enough to be the Asian plate¹⁸. Its interpretation remains enigmatic.

The crustal conductivity structure in our model exhibits marked vertical offsets beneath the surface traces of the Tanggula thrust system (TTS) and the JRS (Fig. 2). Lateral variation in conductivity

observed in the conductive layer can be the result of changes in porosity within the layer, in layer thickness, in the degree of melting and in the degree of interconnectivity of the melt phase²⁰. Surface-elevation homogeneity across the JRS, in contrast to observed irregular Moho geometry^{11,21}, is explained by weak

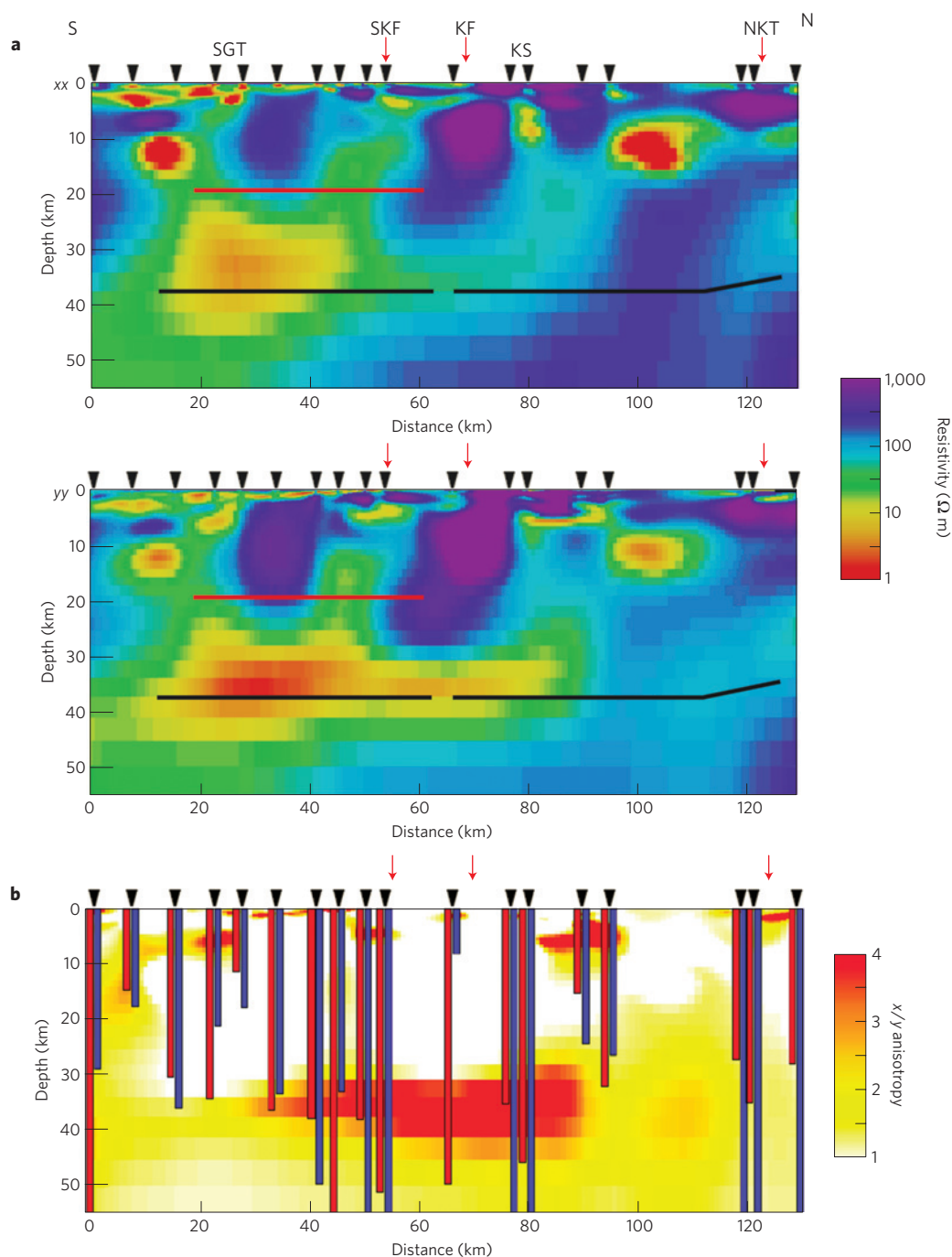


Figure 3 | Local crustal anisotropic 2D modelling. a, 2D crustal anisotropic resistivity model. Only periods lower than 1,000 s were considered for the crustal model. The final RMS misfit of the inversion is 1.94. Two seismic reflectors highlight the top (red line) and the bottom (black line) of a relative low-seismic-velocity layer²⁵. **b**, Anisotropic differences between the xx and yy models. It highlights the conductor extension observed in the yy model beneath the Kunlun Shan. The approximate Niblett–Bostick penetration depths³⁰ of the transverse electric (red) and transverse magnetic (blue) modes are shown in **b**. Abbreviations as in Fig. 2.

middle–lower crust, mapped by the magnetotelluric model, that decouples crust–mantle boundary deformation. This decoupling is characterized by the offset observed in the conductive layer across the suture (Fig. 2). North of the Tanggula Shan, a similar behaviour is observed across the TTS. During the Eocene, the TTS may have played a major role in the uplift of the early Tibetan plateau²², in association with the reactivation of the JRS²³. The Tibetan plateau probably grew through major thrust systems such as the TTS (ref. 22), with the modern equivalent being the North Kunlun Thrust (NKT; Fig. 1) bounding the northern edge of the

plateau with a major drop in elevation. The decoupling of the deformation, generated by the presence of a weak middle–lower crust, associated with the step-by-step thickening of the crust²¹, probably contributed to the atypical topography of the plateau.

To test the anisotropic feature observed on our new 600-line 2D anisotropic inversion model (Figs 2 and 3), 3D synthetic modelling²⁴ (Fig. 4) was undertaken to systematically study magnetotelluric sensitivity to the 3D resistivity transition between the Songpan–Ganzi and the more resistive eastern Kunlun–Qaidam block. The presence of melt was modelled by adding a conductive

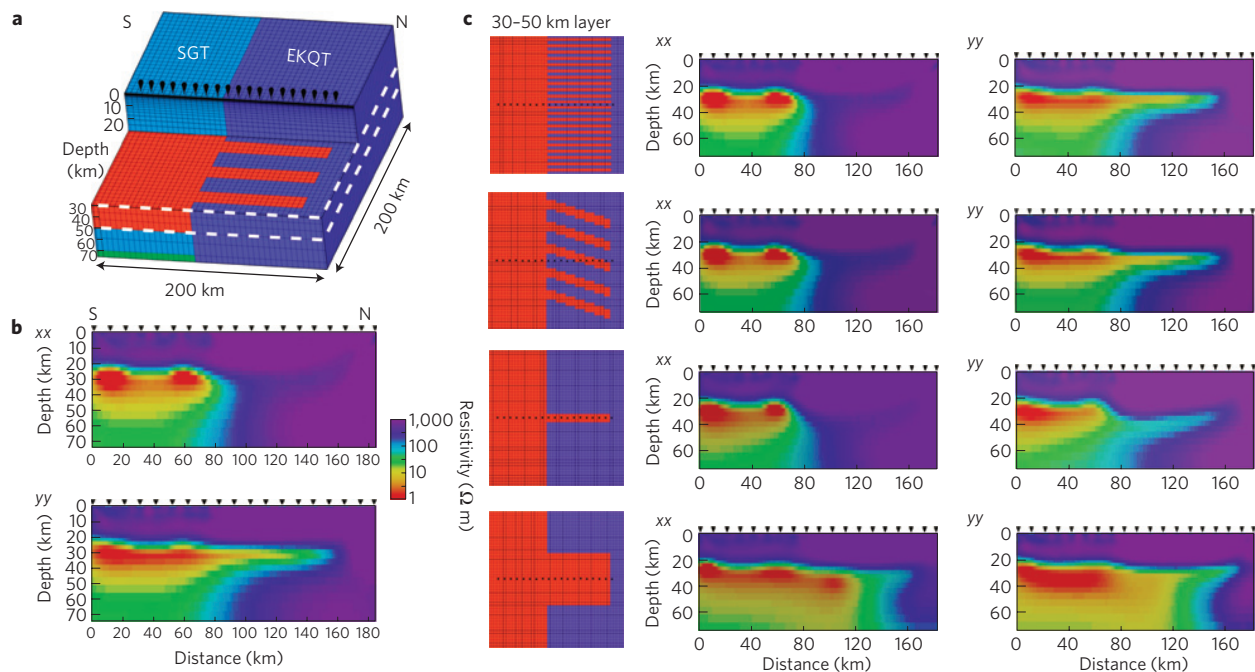


Figure 4 | 3D synthetic modelling associated with 2D anisotropic inversion. **a**, 3D forward model (5×5 km horizontal gridding). The 3D synthetic data were generated for 19 stations using WinGLink²⁴ and random noise was added to the synthetic apparent resistivity (5%) and phase (1.5°) independently. EKQT, eastern Kunlun–Qaidam terrane; SGT, Songpan–Ganzi terrane. **b**, 2D anisotropic inversion model associated with the model in **a**. The synthetic data were inverted with the same 2D anisotropic inversion⁹ as the observed data. **c**, Four alternatives to the model in **a** (only the 30–50 km layer differs) and the corresponding 2D anisotropic inversions.

layer in the middle crust. Different types of 3D melt intrusion penetrating into the most resistive block are simulated (Fig. 4) to account for the anisotropic feature observed in the new models. The anisotropic inversion⁹ was applied on the synthetic forward responses generated by the 3D models (Fig. 4). The inversion results show that our 600-line observations are more likely to be corroborating an anisotropic feature characterized by finger-shaped melt intrusions in contrast to a single intrusion. However, the width, thickness and deviations in the orientation of those finger-shaped intrusions cannot be resolved at the observed depths.

Our anisotropic modelling highlights a transgressive, penetrative extension of the mid-crustal conductive anomaly to the north, crossing the upper-crustal sharp resistivity contrast characterizing the subvertical Kunlun Fault (Fig. 3). Furthermore, the crustal model shows that the anisotropic structure is consistent with wide-angle seismic data²⁵ (Fig. 3). According to our 3D synthetic modelling (Fig. 4), the anisotropic conductive anomaly is likely to be a finger-like manner of melt intrusion beneath the Kunlun Shan. These melt intrusions in the Kunlun middle crust may have been triggered by strain heating²⁶. The weak middle crust crossing the Kunlun Fault is likely to be locally decoupling the upper-crust deformations from the lower crust and mantle. In partially molten rocks, the strength of the rock is mainly controlled by the degree of interconnection of melt. Therefore, as the greatest strength drop occurs for low-melt fractions (<7%; ref. 27), these have a significant effect on rock rheology. This shows that low-melt fractions intrusions would be sufficient to change the rheology of the Kunlun crust. The weaker Kunlun crust thickens vertically in response to the crustal shortening between India and the more rigid Asian blocks represented here by the Qaidam Basin, leading to a Moho offset at the Kunlun–Qaidam border²⁸. The finger-like penetrative melt extension to the north, weakening the Kunlun crust, stops at this offset at the present time²⁵. However, the anisotropy anomaly may not be homogeneous along the whole of the northern Tibetan border and its depth and horizontal

extension to the north is likely to vary. In addition to the eastward crustal flow in eastern Tibet²⁹ characterizing the east–west extension of the plateau, the melt penetration across the Kunlun Fault is accommodating crustal shortening in northern Tibet but may also characterize the growth of the plateau¹⁰ to the north, with extension of the crustal thickening to the south of the Qaidam Basin²⁵.

Methods

The 2D magnetotelluric isotropic modelling approximation assumes that resistivity does not vary perpendicularly to the profile direction. However, the profile orientation defined by the positions of the stations is not necessarily in the correct orientation for this 2D approximation. Furthermore, galvanic distortion effects associated with local 3D inhomogeneities need to be removed also. The strike analysis or distortion decomposition was applied to all stations and frequencies simultaneously to obtain a robust estimation of the regional geo-electric strike and remove the galvanic distortion effects owing to local 3D structures¹⁴. Once the geo-electric strike is estimated, the regional data are derived according to the strike direction and the stations are projected on a profile perpendicular to the strike orientation. The along-strike currents characterize the 2D transverse electric mode and the vertical magnetic field response functions, whereas across-strike currents are associated with the 2D transverse magnetic mode. As the geo-electric strike is characteristic of the global orientation of the 2D regional structures from the upper crust down to the upper mantle, it may differ from the geology strike observed at the surface. Our strike analyses led us to adopt $N85^\circ E$ as the global profile (Fig. 2) geo-electric strike and $N75^\circ E$ as the focused profile (Fig. 3) geo-electric strike, which is in agreement with the east–west trend of the main geological structures.

The 2D anisotropic approximation⁹ operates similarly to the 2D isotropic approximation, but assumes the conductivity varies along anisotropy axes defined as parallel and perpendicular to the main axis of the regional geo-electric strike. The anisotropic inversion code seeks suitable models with an imposed regularization constraint on the closeness of the three models in the three directions⁹ (xx horizontal resistivity across-profile, yy horizontal resistivity along-profile, and zz vertical resistivity). For isotropic inversion, the closeness is set to a high value (100,000) resulting in three models that are identical. For all anisotropic models, the models closeness used was 1, except a value of 0.3 was used for the anisotropic crustal model. Furthermore, for the global and crustal models, the error floors of 8%–3% and 10%–3% were respectively applied for transverse magnetic and transverse electric apparent resistivity and phase, as well as 0.1 for the geomagnetic transfer function for the inversions. The smoothness trade-off lambda used was 1.

Received 13 February 2012; accepted 19 March 2012;
published online 22 April 2012

References

- Jordan, T. A. & Watts, A. B. Gravity anomalies, flexure and the elastic thickness structure of the India-Eurasia collisional system. *Earth Planet. Sci. Lett.* **236**, 732–750 (2005).
- Fan, G. W. & Lay, T. Strong Lg wave attenuation in the northern and eastern Tibetan plateau measured by a two-station/two-event stacking method. *Geophys. Res. Lett.* **30**, 1530 (2003).
- Owens, T. J. & Zandt, G. Implications of crustal property variations for models of Tibetan plateau evolution. *Nature* **387**, 37–43 (1997).
- Unsworth, M. *et al.* Crustal and upper mantle structure of northern Tibet imaged with magnetotelluric data. *J. Geophys. Res.* **109**, B02403 (2004).
- Wei, W. *et al.* Detection of widespread fluids in the Tibetan crust by magnetotelluric studies. *Science* **292**, 716–719 (2001).
- Ding, L., Kapp, P., Zhong, D. L. & Deng, W. M. Cenozoic volcanism in Tibet: Evidence for a transition from oceanic to continental subduction. *J. Petrol.* **44**, 1833–1865 (2003).
- Chung, S. L. *et al.* Tibetan tectonic evolution inferred from spatial and temporal variations in post-collisional magmatism. *Earth Sci. Rev.* **68**, 173–196 (2005).
- Klemperer, S. L. in *Channel Flow, Ductile Extrusion and Exhumation in Continental Collision Zones* Vol. 268 (eds Law, R. D., Searle, M. P. & Godin, L.) 39–70 (Geological Society Special Publications, 2006).
- Baba, K., Chave, A. D., Evans, R. L., Hirth, G. & Mackie, R. L. Mantle dynamics beneath the East Pacific Rise at 17° S: Insights from the Mantle Electromagnetic and Tomography (MELT) experiment. *J. Geophys. Res.* **111**, B02101 (2006).
- Medvedev, S. & Beaumont, C. in *Channel Flow, Ductile Extrusion and Exhumation in Continental Collision Zones* Vol. 268 (eds Law, R. D., Searle, M. P. & Godin, L.) 147–164 (Geological Society Special Publications, 2006).
- Wittlinger, G. *et al.* Seismic tomography of northern Tibet and Kunlun: Evidence for crustal blocks and mantle velocity contrasts. *Earth Planet. Sci. Lett.* **139**, 263–279 (1996).
- Yin, A. & Harrison, T. M. Geologic evolution of the Himalayan–Tibetan orogen. *Annu. Rev. Earth Planet. Sci.* **28**, 211–280 (2000).
- Chen, L. *et al.* Electrically conductive crust in southern Tibet from INDEPTH magnetotelluric surveying. *Science* **274**, 1694–1696 (1996).
- McNeice, G. W. & Jones, A. G. Multisite, multifrequency tensor decomposition of magnetotelluric data. *Geophysics* **66**, 158–173 (2001).
- Rodi, W. & Mackie, R. L. Nonlinear conjugate gradients algorithm for 2-D magnetotelluric inversion. *Geophysics* **66**, 174–187 (2001).
- Jones, A. G. Imaging the continental upper mantle using electromagnetic methods. *Lithos* **48**, 57–80 (1999).
- Partzsch, G. M., Schilling, F. R. & Arndt, J. The influence of partial melting on the electrical behavior of crustal rocks: Laboratory examinations, model calculations and geological interpretations. *Tectonophysics* **317**, 189–203 (2000).
- Zhao, W. *et al.* Tibetan plate overriding the Asian plate in central and northern Tibet. *Nature Geosci.* **4**, 870–873 (2011).
- Arnaud, N. O., Vidal, P., Tapponnier, P., Matte, P. & Deng, W. M. The high K₂O volcanism of northwestern Tibet: Geochemistry and tectonic implications. *Earth Planet. Sci. Lett.* **111**, 351–367 (1992).
- Li, S. *et al.* Partial melt or aqueous fluids in the mid-crust of southern Tibet? Constraints from INDEPTH magnetotelluric data. *Geophys. J. Int.* **153**, 289–304 (2003).
- Vergne, J. *et al.* Seismic evidence for stepwise thickening of the crust across the NE Tibetan plateau. *Earth Planet. Sci. Lett.* **203**, 25–33 (2002).
- Wang, C. *et al.* Constraints on the early uplift history of the Tibetan plateau. *Proc. Natl Acad. Sci. USA* **105**, 4987–4992 (2008).
- Roger, F. *et al.* An Eocene magmatic belt across central Tibet: Mantle subduction triggered by the Indian collision? *Terra Nova* **12**, 102–108 (2000).
- Mackie, R. L., Smith, J. T. & Madden, T. R. Three-dimensional electromagnetic modeling using finite difference equations: The magnetotelluric example. *Radio Sci.* **29**, 923–935 (1994).
- Karplus, M. S. *et al.* Injection of Tibetan crust beneath the south Qaidam Basin: Evidence from INDEPTH IV wide-angle seismic data. *J. Geophys. Res.* **116**, B07301 (2011).
- Whittington, A. G., Hofmeister, A. M. & Nabelek, P. I. Temperature-dependent thermal diffusivity of the Earth's crust and implications for magmatism. *Nature* **458**, 319–321 (2009).
- Rosenberg, C. L. & Handy, M. R. Experimental deformation of partially melted granite revisited: Implications for the continental crust. *J. Metamorph. Geol.* **23**, 19–28 (2005).
- Shi, D., Shen, Y., Zhao, W. & Li, A. Seismic evidence for a Moho offset and south-directed thrust at the easternmost Qaidam–Kunlun boundary in the northeast Tibetan plateau. *Earth Planet. Sci. Lett.* **288**, 329–334 (2009).
- Bai, D. *et al.* Crustal deformation of the eastern Tibetan plateau revealed by magnetotelluric imaging. *Nature Geosci.* **3**, 358–362 (2010).
- Jones, A. G. On the equivalence of the 'Niblett' and 'Bostick' transformations in the magnetotelluric method. *J. Geophys.* **53**, 72–73 (1983).

Acknowledgements

We would like to thank the Science Foundation of Ireland for the financial support (grants 08/RFP/GEO1693 and 07/RFP/GEOF759 to A.G.J.) and M. Unsworth and the other members of the INDEPTH magnetotelluric team from China, USA, Canada and Ireland.

Author contributions

F.L.P. reanalysed, modelled and interpreted the data and wrote the paper. A.G.J. interpreted the data and wrote the paper. J.V. interpreted the data. W.W. designed the project.

Additional information

The authors declare no competing financial interests. Supplementary information accompanies this paper on www.nature.com/naturegeoscience. Reprints and permissions information is available online at www.nature.com/reprints. Correspondence and requests for materials should be addressed to F.L.P.